Int. J. Mech. Sci. Vol. 22, pp. 367–377
Pergamon Press Ltd., 1980. Printed in Great Britain

A FINITE ELEMENT ANALYSIS OF THE RIGID-PLASTIC DEFORMATION OF THE FLANGE IN A DEEP-DRAWING PROCESS BASED ON A FOURTH-DEGREE YIELD FUNCTION—II.

M. GOTOH

Department of Precision Mechanical Engineering, Faculty of Engineering, Gifu University, Kakamigahara-City, 504, Japan

(*Received* 16 *May* 1979; *in revised form* 30 *October* 1979)

Summary—Deformation of the flange in the cylindrical cup drawing process is analysed by the newley-designed hybrid rigid-plastic finite element method on the basis of a fourth-degree yield function f for orthotropy, and the results are compared with those based on the traditional quadratic yield function g and the experiments. The accuracy and the efficiency of the adopted method, the computability of accurate ear-development up to 8-ears by the use of f, the deficiencies in g, relationship between the ear configuration and the planar distribution of r-value and uniaxial yield stress, the factors influencing on the circumferential distribution of drawing force, the effects of various material properties on the degree of ear-development and so forth are demonstrated.

1. INTRODUCTION

In the previous paper[1] (referred as (I) hereafter), a newly-designed finite element formulation for deformation analysis of rigid-plastic materials with orthotropy expressed by a fourth-degree yield function and a few numerical examples of deformation of the flange in a deep-drawing process were demonstrated. However, in those examples, two simplified procedures were utilized for convenience with respect to the subdivision of the flange into triangular finite elements and the removal of the region drawn into the area of the die cavity. In this sense, the data reported in (I) were somewhat inaccurate in the detail.

In this paper, some improvements to these two points are contrived. Then, on the basis of the fourth-degree yield function f, several numerical examples of ear-development of 4, 6 and 8-ears metal sheets are presented, which are compared with the corresponding results based on the quadratic yield function g and the experimental ones. The distribution of drawing force along the die throat periphery (the inner boundary of the modelled flange) and influences of various material properties and initial blank diameter D_0 on the degree of ear-development are also investigated.

Throughout this paper, it is assumed that the initial orthotropy is invariable during deformation, and that the effect of rotation of the principal axes of the orthotropy due to material element rotation with deformation and frictional force between blank and tools on the deforming shape of the flange and the drawing force distribution are negligible.

The first assumption requires that the hardening property of the material is isotropic, or at least that the yield surface of each element undergoing deformation of the same hardening-level stays in contact (at the loading point) with the surface which represents the assumed (isotropically hardened) yield surface. This assumption may be valid restrictively for nearly proportional loadings.

2. THE FOURTH-DEGREE YIELD FUNCTION f

As the author has discussed in detail in the Refs. [2, 3], the fourth-degree yield function expressing orthotropy utilized here possesses the following form with respect to the rectangular cartesian coordinates (x, y) and with the usual notations of stresses;

$$f = \bar{\sigma}^4 = A_1\sigma_x^4 + A_2\sigma_x^3\sigma_y + A_3\sigma_x^2\sigma_y^2 + A_4\sigma_x\sigma_y^3 + A_5\sigma_y^4 + (A_6\sigma_x^2 + A_7\sigma_x\sigma_y + A_8\sigma_y^2)\tau_{xy}^2 + A_9\tau_{xy}^4, \quad (1)$$

where $\bar{\sigma}$ is the equivalent stress, A_7–A_9 are the orthotropy coefficients. x- and y-axes are taken to be coincident with R.D. (the rolling direction) and T.D. (the transverse direction), respectively. On the concepts of the equivalent stress $\bar{\sigma}$ and the corresponding equivalent strain $\bar{\epsilon}$ (or its increment $\overline{d\epsilon}$) defined here should be referred to the Refs.[2, 3]. Taking A_1 to be equal to unity, the relation between $\bar{\sigma}$ and $\bar{\epsilon}$, i.e.

the work-hardening characteristics of the sheet metal, is represented by that between tensile stress σ and longitudinal strain ϵ_l in uniaxial tensile test in R.D., which is expressed as follows;

$$\bar{\sigma} = \sigma_0\{1 + (\bar{\epsilon}/\epsilon_0)\}^n, \tag{2}$$

where σ_0 is the initial yield stress, ϵ_0 and n are the material constants of the metal. Here ϵ_0 is taken to be 0·008. The formulae to determine the coefficients A_2–A_9 are also given in the Ref. [2]. (The author wishes to note that A_3 on the r.h.s. of the equation (55) in the Ref. [2] should be omitted. This is, of course, soley a misprint).

As referred to in the Ref. [2], Hill[4] once discussed generally about a polynomial yield function of arbitrary higher order which includes f, and Bourne and Hill[5] examined the effectiveness of a third-degree yield function.

3. SPECIMENS AND DEEP-DRAWING TEST

The sheet metals tested here are a rimmed-steel (R.S.) and two kinds of aluminium-killed steel (K.S. 1 and K.S. 2) whose nominal thickness is commonly 0·8 mm. R.S. and K.S. 1 yield 4 ears, while K.S. 2 does 6 ears in cylindrical cup-drawing tests. In Table 1, their material constants evaluated from quasi-static experiments are tabulated, where, in this table, r_α is r-value, $X_\alpha (= \sigma_\alpha/\sigma_{RD})$ is the ratio of uniaxial yield stress σ_α to that for R.D. both of which are determined at $\bar{\epsilon} = \epsilon^* = \ln(1{\cdot}15)$, where the suffix α denotes in degree the tensile direction to R.D. X^* equals σ_b/σ_{RD} at $\bar{\epsilon} = \epsilon^*$, where the equi-biaxial yield stress σ_b is evaluated from a hydraulic bulging test. In Table 2, the orthotropy coefficients of each metal calculated by the formulae (53)–(56) in the Ref.[2] are tabulated. In this table, the coefficients of the quadratic yield function g are also given which is squared for convenience of comparison with the fourth-degree yield function f. For a test calculation of 8-ears formation, an artificial test specimen (T.S.) is also considered and listed whose coefficients are designed to yield 8-ears. The figures in parentheses are estimated from others with the aid of some appropriate relations.

In Fig. 1 (a)–(c), the planar theoretical[2] and experimental distributions of r-value are illustrated for the three sheet metals. This figure shows that the theoretical curves based on both of the two yield functions agree well with the experimental ones for all metals. In Fig. 2 (a)–(c), similar illustrations are given with respect to σ_α. From this figure it is seen that, in contrast with r-value, the curves calculated from the yield function g deviates from the experimentals, whereas those based on the fourth-degree yield function f again agree well with them[3].

The substantial meaning of this comparison (Fig. 2) is given in the Ref. [2, 3]. The strain $e_l = 0{\cdot}15$ is chosen for the sake of reference in relation to the following numerical results in which large strain commonly takes place.

As for R.S., K.S. 1 and K.S. 2, quasi-static deep-drawing tests are performed using a hemispherical headed punch of 40 mm diameter, a die of 3 mm die-radius and 42.2 mm die throat diameter, and lubricants of rosin applied at the punch head area and of mixed graphite-tallow (1–3 in weight ratio) at the flange area. The constant blank-holding force is chosen to be twice the value calculated from Siebel's formula[6]. First, the limiting drawing blank diameter (L.D.D.) for each specimen is determined. The test diameter D_0 is set to be a little less than L.D.D. Then, for each sheet metal, incremental partial drawing operations are performed with about 10 hits in total.

The determined values of D_0 are 95 mm for R.S. and 98 mm for both K.S. 1 and K.S. 2. And for T.S. D_0 is chosen to be 95 mm.

The finite element formulation and other basic equations, and calculation procedures except the two points mentioned in the Introduction are all the same as those in (I) and thus nothing about them is repeated here.

TABLE 1. MATERIAL CONSTANTS

material	σ_0 $\frac{kg}{0mm^2}$	n	r_0	$r_{22.5}$	r_{45}	$r_{67.5}$	r_{90}	$X_{22.5}$	X_{45}	$X_{67.5}$	X_{90}	X^*	E_n
R.S.	19.3	0.245	1.21	1.13	1.09	(1.32)	1.50	0.990	1.008	(1.020)	1.006	1.129	4
K.S.1	10.7	0.235	1.85	1.66	1.53	(1.98)	2.38	1.012	1.029	(1.017)	1.002	1.296	4
K.S.2	16.0	0.247	1.70	1.72	1.94	(2.10)	2.30	1.004	0.990	(0.985)	0.989	1.284	6
T.S.	20.0	0.200	1.50	(1.22)	1.50	(1.22)	1.50	1.029	1.000	1.029	1.000	1.050	(8)

E_n = number of ears, R.S. = rimmed steel, K.S.1 & K.S.2 = killed steels, T.S. = trial specimen

TABLE 2. ORTHOTROPY COEFFICIENTS

material	degree of yeild func.	A_2	A_3	A_4	A_5	A_6	A_7	A_8	A_9
R.S.	4	-2.19	3.18	-2.34	0.98	6.73	-6.19	5.64	8.69
	2	-2.19	3.03	-2.01	0.84	5.20	-5.67	4.75	6.75
K.S.1	4	-2.60	3.75	-2.79	0.99	6.29	-7.72	6.33	8.96
	2	-2.60	3.53	-2.39	0.85	5.06	-6.57	4.67	6.41
K.S.2	4	-2.52	3.75	-2.91	1.05	6.24	-8.38	7.28	11.20
	2	-2.52	3.39	-2.27	0.81	6.03	-7.58	5.44	9.09
T.S.	4	-2.40	3.62	-2.40	1.00	4.62	-4.48	4.62	10.42

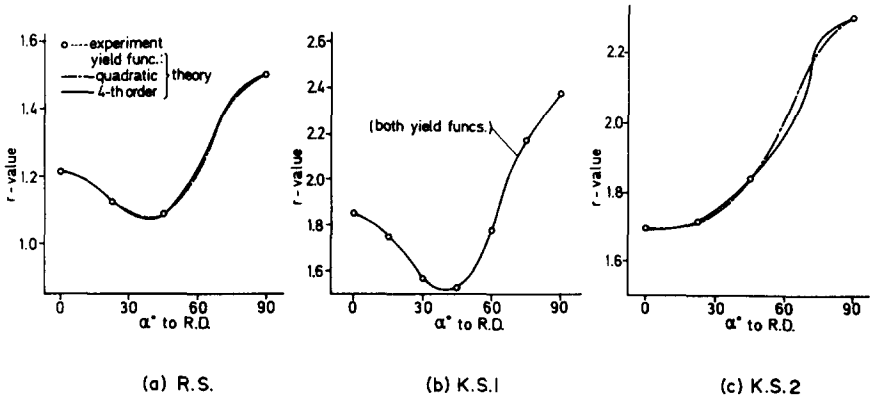

FIG 1. Planar distribution of r-value.

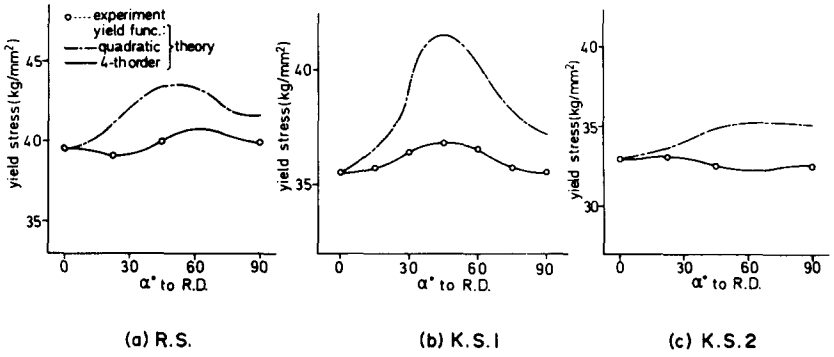

FIG. 2. Planar distribution of uniaxial yield stress σ_α (at nominal longitudinal strain $e_l = 0{\cdot}15$).

4. ELEMENT SUBDIVISION AND BOUNDARY CONDITIONS

The flange region is replaced by a circular plate with a concentric hole of diameter 40 mm (= the punch diameter). Then, in the undeformed state, it is subdivided into a number of triangular finite elements of two types as shown in Fig. 3. The global stiffness matrix is evaluated as the average of those for both of the solid and broken line triangular element-subdivisions. The values of stresses, strains, strain increments and so on are also averaged within each quadrilateral element. Thus the final data for each stage are obtained with respect to each quadrilateral element composed of two triangular elements possessing a common oblique line.

In (I), only the solid line subdivision in Fig. 3 was utilized. However, from an analysis with respect to an *isotropic* sheet metal by the use of this element subdivision, it is found that the deformed shape of the flange becomes *a little* elliptic with its major axis on T.D., and that the distribution of drawing force along the inner periphery shows an abnormal peak and drop at R.D. and T.D., respectively, as seen in Fig. 6 in (I). On the other hand, when both of the two types of element subdivision are utilized, the axi-symmetry of the shape of the deformed flange and the distribution of drawing force is confirmed to hold within the accuracy of computation.

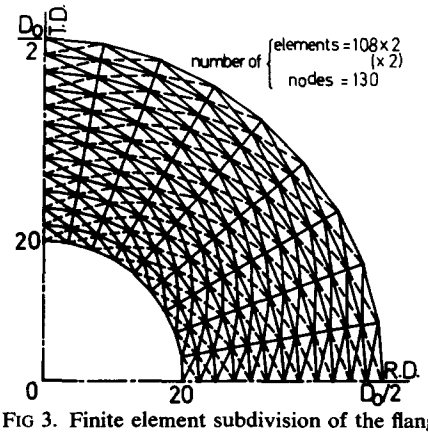

FIG 3. Finite element subdivision of the flange.

Along the inner boundary, a uniform radial displacement increment δu is given at each step of calculation, where its magnitude is chosen to be 0·25 mm at the first step and 0·5 mm thenceforth. The outer boundary is set free from any external force.

As deformation proceeds, the inner portion of the material is inevitably brought into the area of the die cavity. Thus such a portion of the material is cut off and excluded from calculation in the following steps. Then new nodal points (with equi-distance) are set along each radial line by re-subdividing the line between the nodal point on the outer boundary and the corresponding one on the inner boundary. Namely, an element re-subdivision technique is designed at each step. The number of the division along a radial line is reduced by 1 per 10 steps. Before proceeding to the next step, physical quantities such as stresses, strains, thickness etc. in each newly produced element are also re-evaluated from those in all the old ones which are partially occupied by it, taking their volume-weighted averages.

In (I), the following simplified method was adopted. The effect of the portion of the flange brought into the area of the die cavity was neglected until its amount exceeded some level and then the most-inner element array was cut out at one time when it exceeded that level. Then element re-subdivision was not required and thus such a cumbersome skill in computation as described above was not necessary. However, the calculated total drawing force was not very accurate and dropped discontinuously after every element-removal. Moreover, the shape of the deformed flange would also be affected significantly by this simplified procedure with deformation. In this paper, in most cases, drawing process will be pursued upto the end of drawing (i.e. until one of nodal points on the outer boundary reaches the inner boundary), and thus this simplified technique cannot be adopted.

Computations in this paper are performed by the use of the computer FACOM 230-75 at Nagoya University Computation Center. The CPU-time for one blank with $D_0 = 90 \sim 98$ mm is 15–20 min and total steps are 70–90. The magnitude of strain extends over a range of 0–1·5 throughout the following numerical examples.

5. RESULTS AND DISCUSSIONS

(5.1). *Specimens listed in Table* 1

Figs. 4–6 are the results of R.S. Fig. 4 illustrates the patterns of the deformed outer boundary with the total drawn-in length $u = \int \delta u$ as a parameter. The results of calculation based on the quadratic and fourth degree yield functions show 4-ears to agree with the experiment (see Table 1). However, the result by the quadratic one g gives a far greater ear-development than that by the fourth degree one f. Moreover, it is noted that, contrary to the fact, the prediction of ear pattern from the uniaxial yield stress distribution (Fig. 2a) would be 6-ears [2–4]. In this case, the ear pattern seems to be governed by the r-value distribution (Fig. 1a). Or, at least, this example shows that it is not necessarily reliable to deduce the ear-pattern only from the uniaxial yield stress distribution as proposed classically by Hill [2, 4]. Namely, the ear-pattern may be governed by both of the distributions. Fig. 5 illustrates the ear-development E_d with deformation, taking $E_d = \{(D_{max} - D_{min})/2D_0\} \times 100$ as the ordinate and u as the abscissa, where D_{max} and D_{min} are the maximum and minimum current outer diameters, respectively. This figure includes also the corresponding experimental curve. From this figure, it is found that the result based on f agrees well with that of the experiment, whereas that due to g is about twice as large as the latter at the final stage of drawing (see Refs. [1, 7–10].

Fig. 6 illustrates the distribution of drawing force along the inner periphery with u as a parameter. In general, there would be the following three factors influencing on it; (a) The planar distribution of r-value. (The drawing force is expected to be larger in the direction of smaller r-value.) (b) The planar distribution of uniaxial yield stress σ_α. (Following Hill [2, 4], the distribution of drawing force would depend on that of σ_α with replacement α by $(90°-\alpha)$.) (c) The configuration of the deformed flange. (The drawing force is larger in the direction of a higher ear.)

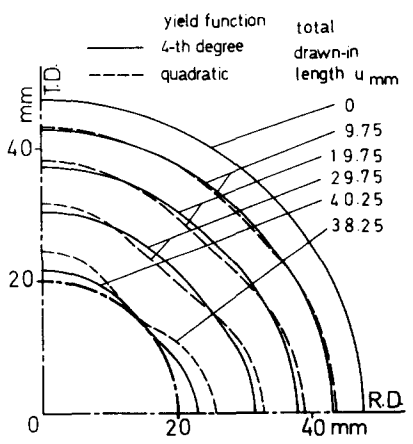

FIG. 4.

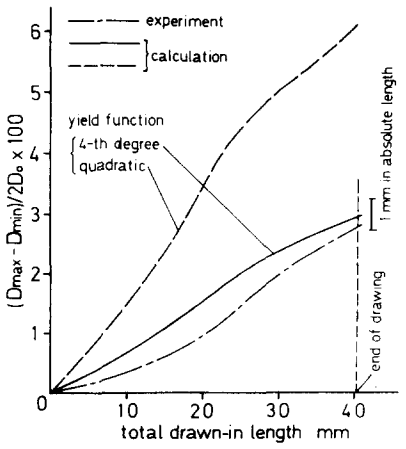

FIG. 5.

FIG 4. Calculated outer boundaries of the deformed flange (R.S.).

FIG 5. Variation of relative ear-height with deformation (R.S.).

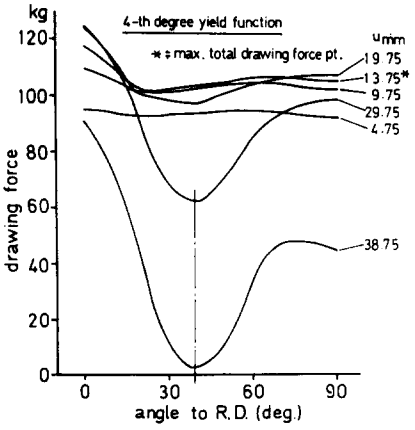

FIG. 6.

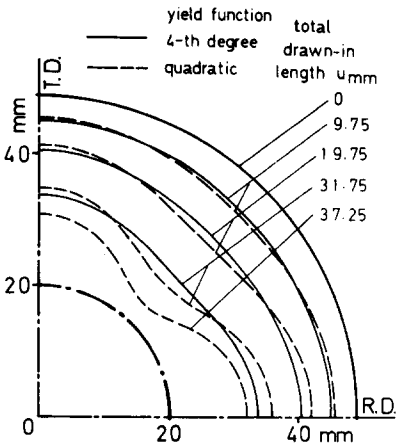

FIG. 7.

FIG. 6. Variation of drawing force distribution along the inner periphery with deformation (calculation; R.S.).

FIG. 7. Calculated outer boundaries of the deformed flange (K.S. 1).

We should note that the influence of (a) and (b) is contrary to that of (c), because an ear is prone to grow in the direction of larger r-value and $90° - (\alpha$ of smaller $\sigma_\alpha)$. In the case of R.S., the distribution of drawing force seems to be dependent on both of (a) and (b) during earlier stage of deformation (see Figs. 1 and 2). However, throughout the whole deformation history, it takes the maximum value at R.D. ($\alpha = 0°$) at which the outer diameter also becomes maximum.

Figs. 7–9 are the results of K.S. 1. Here the computation time is restricted to be 15 min. Figs. 1(b) and 2(b) predict this material to produce 4 ears. Actually it produces 4 ears not only experimentally but also numerically (Fig. 7). K.S. 1 possesses the strongest anisotropy among the three tested metals. It is noted again in Fig. 7 that the quadratic yield function g gives a too excessive ear-development, which is demonstrated more explicitly in Fig. 8 which illustrates E_d vs u curves. Fig. 9 illustrates the distribution of drawing force along the inner periphery. At the first stage of deformation, it takes the maximum value at about 45° due to both effects of the factors (a) and (b). However, drawing force at this direction decreases relatively with deformation, because a hollow is produced here. Then the maximum drawing force occurs at R.D., because the height of the ears and the magnitude of σ_α-s in R.D. and T.D. are comparable and r-value at R.D. is smaller than that at T.D.

Figs. 10–12 are the results of K.S. 2. This material is expected to produce 2 ears from r-value distribution (Fig. 1c) and 6 ears from σ_α-distribution (Fig. 2c), respectively.

Fig. 10 demonstrates that the flange calculated on the basis of the yield function f presents 6 ears in accordance with the experiment (Table 1), whereas that based on g does 4 ears. From Fig. 11, it is found

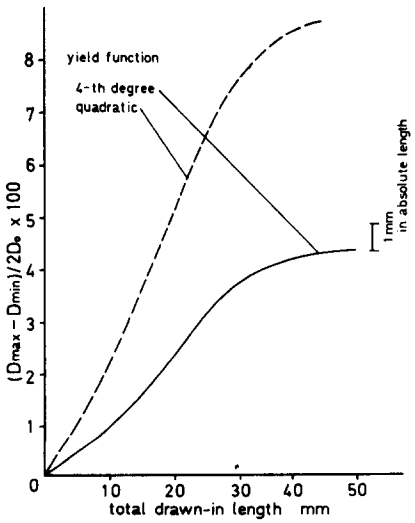

FIG. 8.

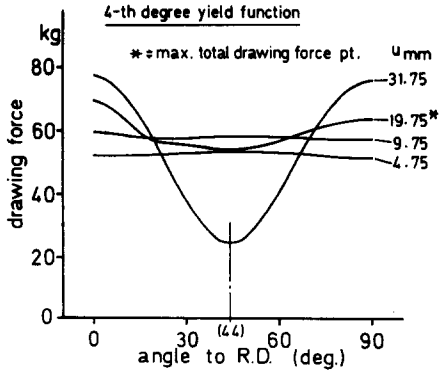

FIG. 9.

FIG. 8. Variation of relative ear-height with deformation (K.S. 1).

FIG. 9. Variation of drawing force distribution along the inner periphery with deformation (calculation; K.S. 1).

that the rate of ear development is well predicted by the calculation based on the yield function f. In contrast with R.S., the calculated ear development is a little less than the experiment. Here the result based on the yield function g is excluded, because its ear configuration is wrong. The distribution of drawing force along the inner periphery is illustrated in Fig. 12. It takes the maximum value at R.D. from the initial step to the step at which the total drawing force reaches its maximum value, though the outer diameter is minimum at R.D. and σ_α is minimum at T.D. This seems due to r-value distribution which increases monotonically with α (see Fig. 1c). In later stage of deformation, the distribution of drawing force is clearly governed by the deformed configuration of the flange.

Fig. 13 illustrates the variation of the total drawing force with u up to the end of drawing with respect to R.S. and K.S. 2. This figure shows that the maximum total drawing force reads 3·81 ton for R.S. and 3·25 ton for K.S. 2. On the other hand, the corresponding experimental values are 4·0 ton and 3·5 ton, respectively, and thus those calculated values are reasonable, because redundant force due to friction and bending is neglected in the calculation.

Figs. 14 and 15 are the results of T.S. in Table 1 or 2 which is expected to produce 8 ears. Only the fourth-degree yield function f is reasonably applied. From Fig. 14, it is verified that development of 8-ears is also well simulated numerically with the aid of this yield function. This material is designed to possess mechanical properties of almost 45°-symmetry (see Tables 1 and 2). The calculated configruation of the deformed flange is certainly so, which verifies the accuracy of the calculation technique adopted here. The distribution of drawing force along the inner periphery illustrated in Fig. 15 is also almost of 45°-symmetry. However, from the initial stage of deformation to the end, drawing force takes higher value at 0°, 45° and 90° in contrast with that expected from r-values and σ_α-s given in Table 1. Namely, in this case, it is exclusively influenced by the pattern of the deformed flange from the instant of the onset of deformation.

(5.2). *Influence of various factors on ear-development*

On the basis of the fourth-degree yield function, various factors influencing on ear-development are investigated with respect to 4-ears-materials. The material properties of K.S. 1 which is a typical 4-ears-material as described in the previous article are modified for this purpose. They are tabulated in Table 3. In this table, the following notations are used;

$$\Delta r = (r_0 + r_{90})/2 - r_{45}, \tag{4}$$

$$\Delta X = (X_0 + X_{90})/2 - X_{45}, \quad X_0 = 1 \tag{5}$$

where $X_\alpha = \sigma_\alpha/\sigma_{RD}$. Δr is the usual planar anisotropy coefficient and ΔX is a similar one for σ_α-distribution. Thus ΔX has its significance only when the fourth-degree yield function is utilized. Furthermore, from the definitions (4) and (5), it should be noted that both of the coefficients Δr and ΔX make sense only for 4-ears-materials. The test specimens Nos. (1)–(8) possess the same initial diameter of 90 mm. No. (1) and Nos. (9)–(11) possess the same material properties as those of K.S. 1.

Fig. 16. illustrates ear-development with deformation up to the end of drawing with respect to the specimens Nos. (1)–(8). (The curve for No. (8) is once cut and then continued from lower part of the ordinate for a sake of convenience.) In this figure, D.R. denotes drawing ratio (= D_0/(the inner diameter)) and thus is equal to 90/40 = 2·5. From this figure, the final relative ear-height $[(D_{max} - D_{min})/2D_0 \times 100]_{final}$ is read for each specimen and, together with the final step of calculation N_{final} and total drawn-in length u_{final} which are both extrapolated exactly to the end of drawing, tabulated in Table 4. The data of the specimens Nos. (9)–(11) are also estimated in the same manner as this and recorded in this table. According to Table 4, influences of various factors on the final relative ear-height (F.R.E.H.) can be inspected.

Fig. 17 illustrates the influence of Δr on F.R.E.H. keeping the other factors unchanged, where the effect of a slight variation of $\bar{r}$ (= average value of r_α) is neglected. From this figure, it is noted that F.R.E.H.

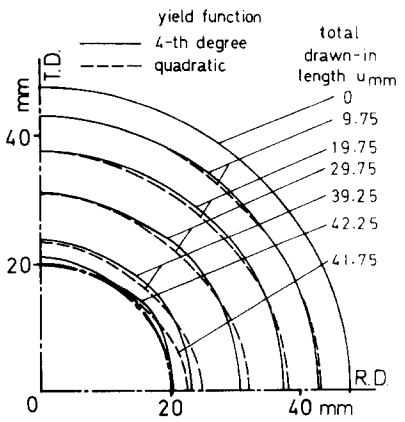

FIG. 10.

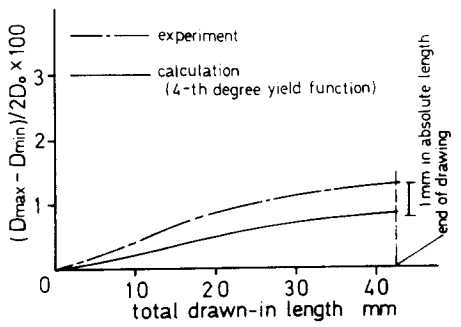

FIG. 11.

FIG. 10. Calculated outer boundaries of the deformed flange (K.S. 2).

FIG. 11. Variation of relative ear-height with deformation (K.S. 2).

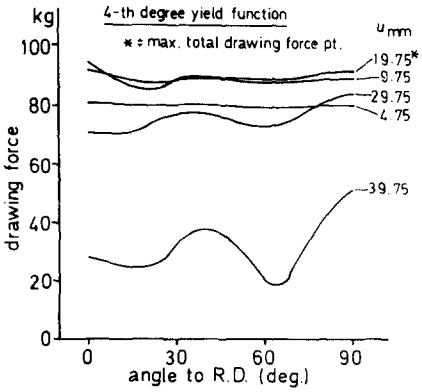

FIG. 12. Variation of drawing force distribution along the inner periphery with deformation (calculation; K.S. 2).

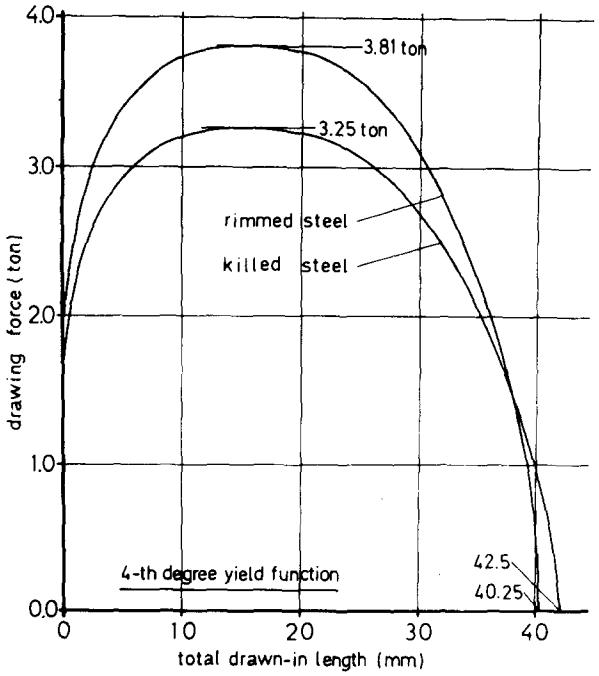

FIG. 13. Variation of total drawing force with deformation (calculation).

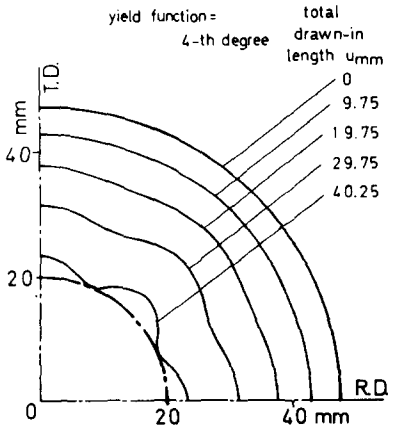

FIG. 14.

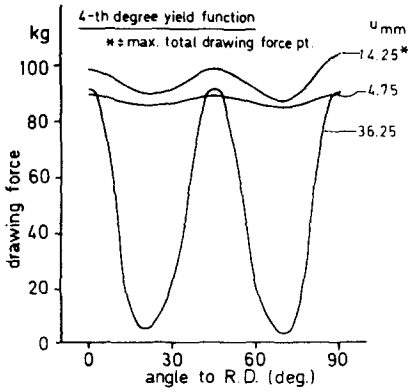

FIG. 15.

FIG. 14. An example of deformed flange with 8 ears (calculation; T.S.).

FIG. 15. Variation of drawing force distribution along the inner periphery with deformation (calculation; T.S.).

TABLE 3. MATERIAL CONSTANTS OF NO. (1) ~ NO. (11)

specimen No.	n	X#	Δr	-ΔX	D_0 (mm)
(1)	0.235	1.296	0.585	0.029	90
(2)	"	"	0.32¥	"	"
(3)	"	"	0.05¥¥	"	"
(4)	"	"	0.585	0.015$	"
(5)	"	"	"	0.000$$	"
(6)	0.100	"	"	0.029	"
(7)	0.235	1.000	"	"	"
(8)	0.010	1.296	"	"	"
(9)	0.235	"	"	"	80
(10)	"	"	"	"	60
(11)	"	"	"	"	98

¥ $r_0 = r_{90} = 1.85$, $r_{45} = 1.53$, $r_{22.5}=r_{67.5}=1.66$,

¥¥ $r_0 = r_{90} = 1.60$, $r_{45} = 1.55$, $r_{22.5}=r_{67.5}=1.58$,

$ $X_{22.5}=X_{67.5}=1.010$, $X_{45}=1.015$, $X_{90}=1.000$,

$$ $X_{22.5}=X_{67.5}=X_{45}=X_{90}=1.000$.

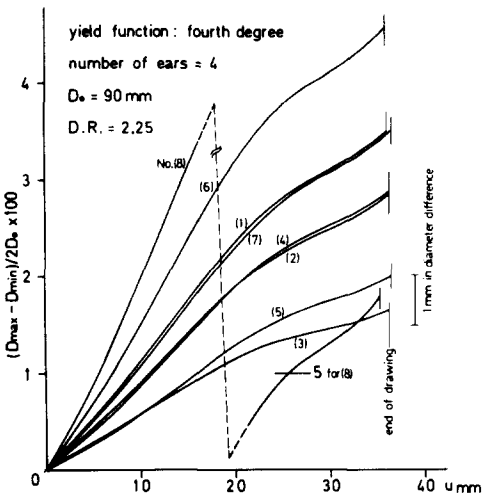

FIG. 16. Variation of relative ear-height with deformation (calculation; specimens Nos. (1) ~ (8)).

TABLE 4. RESULTS OF CALCULATION

specimen No.	N_{final}	$u^{(mm)}_{final}$	F.R.E.H.
(1)	71.71	35.61	3.52
(2)	72.37	35.94	2.87
(3)	72.83	36.17	1.66
(4)	72.39	35.95	2.89
(5)	72.97	36.24	2.01
(6)	71.15	35.33	4.60
(7)	72.74	36.12	3.54
(8)	70.37	35.12	5.79
(9)	53.85	26.68	2.25
(10)	23.77	11.64	0.56
(11)	90.50	45.00	4.63

F.R.E.H. = $[(D_{max} - D_{min})/2D_0 \times 100]_{final}$.

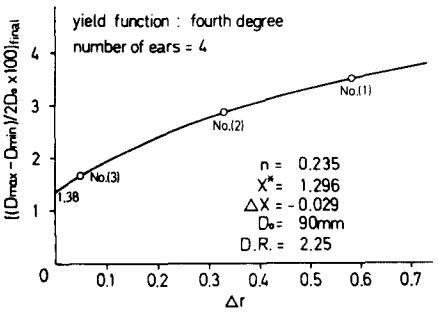

FIG. 17.

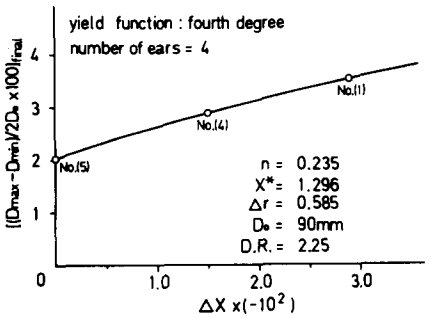

FIG. 18.

FIG. 17. Influence of Δr on F.R.E.H. (calculation).

FIG. 18. Influence of ΔX on F.R.E.H. (calculation).

increases with Δr as usually said, and that the rate of its increase is a little larger for a range of smaller Δr. The value of F.R.E.H. at $\Delta r = 0$ is found to be 1·38 which can be regarded to be its portion due only to ΔX which is rather remarkable. As is readily understood, Δr may be negative. Then the curve would extend smoothly downward to the left up to the Δr-axis and then go up again further to the left like its counterpart on the right.

Fig. 18 illustrates the influence of ΔX on F.R.E.H., where the effect of incidental variation of $\bar{X}$ (= average value of X_α) is neglected. It is seen that a material with larger ΔX produces larger F.R.E.H. and the relation between ΔX and F.R.E.H. is almost linear with a slight convex trend upward. The non-zero value of F.R.E.H. at $\Delta X = 0$ is owing to the effect of Δr. ΔX can be negative, like Δr, and then the curve would extend to the left in a similar manner as just described about Fig. 17.

Fig. 19 illustrates the influence of n on F.R.E.H., where n in the equation (2) is not exactly equal to the so-called n-value (strain-hardening exponent n' in an expression of hardening characteristics $\bar{\sigma} = c\bar{\epsilon}^{n'}$), but it possesses obviously a similar physical meaning as n'. From this figure, it is found that F.R.E.H. is larger for smaller n and, moreover, its variation due to n is very remarkable. The value 5·94 of F.R.E.H. at $n = 0$ (i.e. no work-hardening) is 1·69 times as large as the value 3·52 for K.S. 1 (No. 1). It is well known that materials with hard quality generally produce highest ears. According to Fig. 19, this can be considered not only because they possess strongest planar anisotropy but also because they possess usually smallest n-value.

Fig. 20 illustrates a relation between F.R.E.H. and D.R. or D_0. It is seen that F.R.E.H. increases slowly in the range of smaller D_0 and then rapidly beyond this range. The curve looks parabolic.

Finally, comparing the result of No. (1) with that of No. (7), the influence of variation of X^*-value on F.R.E.H. is confirmed to be almost undetectable.

(5.3). *A remark on influence of variation of anisotropy*

In this report, we have considered the anisotropy of the material to be invariable throughout deformation history. In spite of this simplification, as described in the article (5.1) the ear-height and the total drawing force calculated are confirmed to agree well with the corresponding experimental results. This may be because the state of loading in the flange is nearly proportional or simple. Namely, a remarkable effect of anisotropy variation is considered to occur restrictedly to the case in which subsequent loading takes a path far from that of the preceeding one, because variation of anisotropy is generally appreciated due to the shape change of the yield surface with deformation which is usually severe at the points far from the current loading point on it.

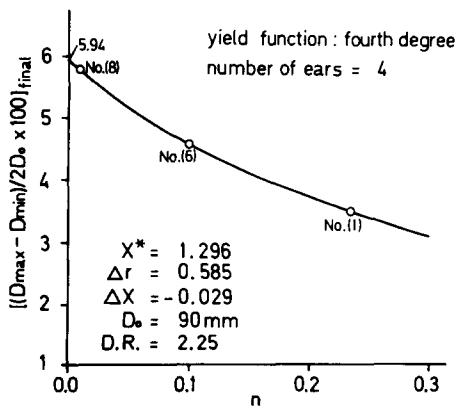

FIG. 19.

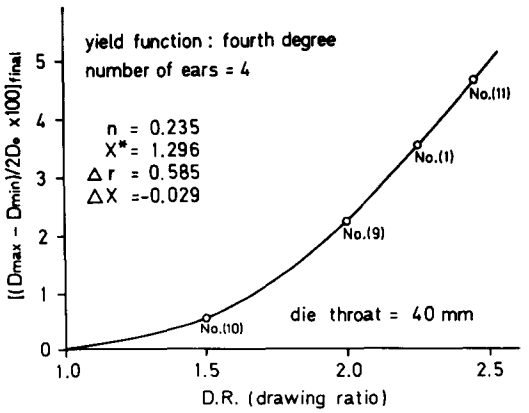

FIG. 20.

FIG. 19. Influence of n on F.R.E.H. (calculation).

FIG. 20. Influence of D_0 on F.R.E.H. (calculation).

Finally, it is noted that, if rotation of the principal axes of orthotopy and frictional force due to the blank-holder both of which are neglected here are taken into consideration, more reliable results would be obtained.

6. CONCLUSIONS

Deformation analyses of the flange with orthotropy in a cylindrical cup-drawing process are performed with the aid of a newly designed rigid-plastic finite element method mainly on the basis of a fourth-degree yield function. The results are summed up as follows;

(1) Irrespective of ear-configuration, deformation of the flange which produces at most 8 ears can be numerically simulated very well up to the end of drawing by the method designed here, including distribution of drawing force along the inner periphery.

(2) The final relative ear-height (F.R.E.H.) can be evaluated within a practical accuracy by this numerical calculation on the basis of the fourth-degree yield function, neglecting the effects of frictional force due to the blank-holder, rotation of the principal axes of orthotropy and variation of anisotropy due to deformation. However, numerical analysis based on the quadratic yield function gives, irrespective of ear-configuration, only inaccurate data.

(3) The orientation of an ear produced depends on both of the pattern of planar distribution of r-value and that of σ_α (= uniaxial yield stress in the direction of α to R.D.) and the magnitude of them. Generally speaking, an ear is prone to grow in the direction of larger r-value or $\{90° - (\alpha$ of smaller $\sigma_\alpha)\}$ and its height depends on their magnitude.

(4) Distribution of drawing force F along the inner periphery is, from the onset of deformation to nearly the step at which the total drawing force takes its maximum value, dependent on (a) the r-value distribution (F is larger for smaller r), (b) the σ_α-distribution with replacement α by $(90° - \alpha)$ (F is larger for larger $\sigma_{90-\alpha}$), and (c) configuration of the deformed flange (F is larger in the direction of a higher ear). However, in later stage of deformation, it becomes dependent only on (c). There may exist those materials whose distribution of F is governed only by (c) throughout deformation history. The 8-ears-material tested here is one of such materials.

(5) As for 4-ears-materials, the values of Δr and ΔX defined by the equations (4) and (5), respectively, are the main factors which govern the magnitude of ear-height. ΔX makes sense only when the fourth-degree yield function is introduced. When $\Delta r > 0$ and $\Delta X < 0$, ears grow at R.D. and T.D. and F.R.E.H. is higher for larger values of Δr and $(-\Delta X)$. According to the data presented here, variation of F.R.E.H. with Δr of range $0{\cdot}0 \sim 0{\cdot}6$ amounts to that with $(-\Delta X)$ of range $0{\cdot}00 \sim 0{\cdot}05$. When $\Delta r < 0$ and $\Delta X > 0$, hollows grow at R.D. and T.D. However, when the sign of ΔX is coincident with that of Δr, a cancellation between the effects of them occurs and ear-configuration may take even a pattern other than 4-ears.

(6) Variation of X^*-value (= equi-biaxial yield stress/σ_{RD}) affects little on F.R.E.H. On the other hand, that of the strain-hardening exponent n influences significantly on F.R.E.H. Namely, F.R.E.H. is larger for a smaller n. An example presented here states that F.R.E.H. extends over the range of $5{\cdot}94 \sim 3{\cdot}52$ for $n = 0{\cdot}000 \sim 0{\cdot}235$, i.e. an ear which is 1·69 times as high as one in a material of $n = 0{\cdot}235$ may be produced in a non-hardening material.

(7) The influence of the initial diameter D_0 or D.R. on F.R.E.H. is also remarkable. A numerical example presented here reports that, for a range of D.R. (= drawing ratio) larger than about 1·6, F.R.E.H. increases rapidly with D_0, though it shows only a slight increase with D_0 for smaller D.R.

REFERENCES

1. M. GOTOH and F. ISHISE, *Int. J. Mech. Sci.* **20**, 423 (1978).
2. M. GOTOH, *Int. J. Mech. Sci.* **19**, 505 (1977).

3. M. GOTOH, *Int. J. Mech. Sci.* **19**, 513 (1977).
4. R. HILL, *Mathematical Theory of Plasticity*, p. 317. Clarendon Press, Oxford (1950).
5. L. BOURNE and R. HILL, *Phil. Mag.* **41**, 671 (1950).
6. E. SIEBEL, *Stahl und Eisen*, **3**, 155 (1954).
7. T. JIMMA, *J. Japan Soc. Tech. Plasticity*, **11**, 707 (1970), (in Japanese).
8. S. KOBAYASHI, C. H. LEE and S. N. SHAH, *J. Japan Soc. Tech. Plasticity*, **14**, 770 (1973).
9. C. H. LEE and S. KOBAYASHI, *Proc. 15th Int. Machine Tool Design and Res. Conf.* Birmingham (1974).
10. J. KIBARA and M. YOSHIDA, *J. Japan Soc. Tech. Plasticity*, **18**, 598 (1977), (in Japanese).